Progress In Electromagnetics Research M, Vol. 120, 41–54, 2023

Lateral Flow Immunoassay Strip Based on Confocal Raman Imaging for Ultrasensitive and Rapid Detection of COVID-19 and Bacterial Biomarkers

Chuan Zhang[1, 2], Anqi Yang[1], and Sailing He[1, 2, 3, 4, *]

Abstract—Rapid and sensitive analysis of proteins in complex biological environments is crucial for the screening and defense against infectious diseases. Here, we show that the lateral flow immunoassay strip based on confocal Raman imaging can achieve immune analysis at pM and $\sim 10^4$ cfu/mL molecular level for the rapid detection of COVID-19 virus and bacteria. Fluorescent dyes of Alexa 647 were used as Raman markers in the Raman silent region of 1800 cm^{-1} and 2800 cm^{-1}, and colloidal gold nanospheres were used to enhance the Raman signal. Raman imaging was performed with our self-developed confocal Raman microscopy for COVID-19 and Escherichia coli O157: H7 on lateral flow immunoassay strip. Compared to traditional colloidal gold test strips, the sensitivity of this technology has been significantly improved. This work will promote the widespread application of surface enhanced Raman detection for bacteria and virus, which is of great significance for *in vitro* screening and disease diagnosis.

1. INTRODUCTION

In complex ecological environments, it is crucial to conduct highly sensitive, low-cost, stable, and rapid immune analysis of proteins [1, 2]. This mainly depends on the following aspects: some protein biomarkers exist at low abundance in the early stages and are difficult to monitor, especially in complex environments, such as various body fluids, daily foods, and waste fluids [3–5]. Currently, many ultrasensitive immune technologies have been developed, such as electrochemical immunosensor [6], single molecule detection [7], microfluidic technology [8], mass spectrometry immunoassay [9, 10], and hyperspectral sensing imaging [11, 12]. However, the high sensitivity of these technologies, such as computed tomography (CT) diagnosis and nucleic acid screening of COVID-19 [13, 14], traditional cultivation and identification of pathogenic microorganisms susceptible to infection in infants [15], and imaging examination of infectious diseases [16], comes at the price of expensive instruments and costs, complex technical operations, and longer detection times, which cannot meet the needs of fast and high-throughput detection. Therefore, it is important to develop some sensitive and rapid detection methods (with relatively low-cost equipment), which meet the above requirements for protein immunoassay.

The lateral flow immunoassay is considered a real-time on-site diagnostic tool that can quickly monitor target proteins without any professional technical support [17–19]. It is assembled from parts such as filters, nitrocellulose filter membrane (NC membrane), sink pads, and backing cards. The basic functions of coupling, analysis, etc. are miniaturized onto a strip of a few square centimeters, completing a series of steps such as sample pretreatment, separation, mixing, chemical reaction, and detection. Among them, the NC membrane is the most important component in the test strip. It serves

Received 11 October 2023, Accepted 20 October 2023, Scheduled 21 October 2023

* Corresponding author: Sailing He (sailing@zju.edu.cn).

[1] Center for Optical and Electromagnetic Research, College of Optical Science and Engineering, Zhejiang University, Hangzhou 310052, China. [2] Taizhou Hospital, Zhejiang University, Taizhou 318000, China. [3] National Engineering Research Center for Optical Instruments, Zhejiang University, Hangzhou 310052, China. [4] Department of Electrical Engineering, Royal Institute of Technology, SE-100 44 Stockholm, Sweden.

as a solid phase carrier and binds to peptide bonds in the antibody through electrostatic interactions, fixing the primary antibody onto the NC membrane. Also, the NC membrane utilizes its porous structure to drive the liquid forward under capillary force, allowing the target in the sample to be captured and detected [20, 21]. At present, colloidal gold test strips are the most traditional method, using gold nanospheres coupled with secondary antibodies to capture targets, and the gold nanospheres are gathered on the test line (T line) and displayed in red [22]. Nowadays, colloidal gold test strips have been widely used in medical diagnosis, food safety, environmental monitoring, etc., Such as, the widely used pregnancy test strip has shortened the detection time from two hours to just a few minutes, and visualized results can be obtained for self-inspection in the home [23]. Allergen proteins such as casein and ovalbumin in food can be quickly and multiplex detected in real-time by modifying different nanoparticles [24]. The serological detection of novel coronavirus antibodies provides useful help for the diagnosis of COVID-19 [25]. This detection method is convenient, efficient, cost-effective, does not require any equipment and professional technical support, and only judges the analysis results with the visual observation within a few minutes. However, such a visual observation results in significant subjective factors affecting the sensitivity and quantitative analysis of this method [26, 27].

To address this issue and improve the sensitivity, various types of lateral flow immunoassays have been developed, such as electrochemistry [28, 29], fluorescence [30, 31], chemiluminescence [32, 33], and Raman spectroscopy [34, 35]. Among them, Raman spectroscopy has attracted much attention due to its ability to provide unique molecular fingerprints of samples [36–39]. However, the Raman signals of most molecules themselves are usually weak, making it difficult to perform trace detection with instruments. Surface enhancement of Raman scattering overcomes the disadvantage of insufficient signal strength and can obtain spectral information that is not easily obtained by conventional Raman spectroscopy [40]. Surface enhancement of Raman scattering is caused by the excitation of surface plasmon resonance around the surface of metallic nanoparticles, which gives the electromagnetic enhancement effect of local electric field concentrated on the 'hot spot' near the metal surface [41, 42]. There have been many reports on the combination of SERS and lateral flow immunoassay strips for detection. For example, Chen et al. [43] proposed a vertical chromatography detection technique based on surface enhanced Raman scattering to detect multiple inflammatory biomarkers at a single test point. This detection technology significantly improves detection sensitivity, demonstrating extremely low background, high stability, and reliability in serum sample analysis. Fu et al. [44] developed a SERS based lateral flow biosensor for simple, fast, and sensitive detection of biomarkers of HIV-1 DNA, achieving high reproducibility in quantitative analysis. Compared with commercial fluorescent reagent kits, it reduces the detection time by three orders of magnitude. Zhang et al. [45] developed a novel multiplex SERS side flow immunosensor for detecting mycotoxins in corn. Compared with enzyme-linked immunosorbent assay (ELISA), its sensitivity has increased by about an order of magnitude. He et al. [46] established a dual mode (colorimetric and SERS) side flow detection method based on platinum coated gold biological nanorods and surface enhanced SERS enhancement properties for the specific detection of *Clostridium jejuni* in food, achieving a wide detection range, low detection limit, high specificity, and excellent sensitivity. Su et al. [47] used metal core-shell Au/Au nanostars as multifunctional labels to conduct dual model colorimetric/SERS side flow immunoassay for residual clenbuterol in food. The constructed detection method has high specificity, high reproducibility, and satisfactory recovery rate in food detection. Liu et al. [48] developed a detection device consisting of a lateral flow immunoassay strip based on surface enhanced Raman scattering for the ultra sensitive quantitative analysis of SP10. This detection method uses gold and silver core-shell nanorods as SERS nano-labels, which has the advantages of high sensitivity, low cost, and very fast analysis processing. The reaction can be completed in only 10 minutes. Although these lateral flow detection technologies based on SERS have advantages such as significantly improving detection sensitivity, they also have some shortcomings. Most of these reported results used conventional Raman spectroscopy systems to perform SERS measurement point by point (instead of imaging over an area), which may lead to random errors that affect the detection accuracy. Moreover, the characteristic wavelengths of the Raman probes used in these reports range from $600\,\mathrm{cm}^{-1}$ to $1800\,\mathrm{cm}^{-1}$, and many substances produce Raman signals, resulting in measurement errors. However, using Raman probes with characteristic peaks in the silent region can overcome this drawback well. The Raman silent region is the wavenumber range in the Raman spectrum where there is no or little Raman scattering signal, usually between $1800\,\mathrm{cm}^{-1}$ and $2800\,\mathrm{cm}^{-1}$. The existence of the Raman silent

region is due to the selection rules and symmetry of the molecular vibrational modes. In the Raman silent region, using specific Raman probes can achieve high sensitivity and specificity for the detection of target molecules, avoiding the interference of other molecules. The study by He et al. [49] showed that Confocal Raman Microscopy (CRM) can provide information about the composition and distribution of biomolecules in biological samples in an *in situ*, label-free, and non-destructive manner with high spatial resolution. They also found that using different preservation methods has specific effects on CRM imaging and signal results. The study by Hu et al. [50] proposed a compressive imaging strategy that combines context-aware imaging priors to improve Raman imaging speed while maintaining the traditional advantages of point scanning imaging such as isotropic resolution and confocal resolution. This method can reduce the number of measurements by about 85% while maintaining high image quality (SSIM > 0.85). Using confocal Raman imaging can obtain a larger data set in a shorter time to obtain more reliable downstream analysis results.

In this study, we constructed a highly sensitive and a home-made confocal Raman imager. Compared to a spectral imager [51] and a hyperspectral imager [52], a confocal Raman imager has a much higher spectral resolution (typically better than 1 nm). The confocal feature would enable us to achieve a higher signal-to-noise ratio by filtering out the interference information in the neighboring non-focus area [53, 54]. Consequently, better sensitivity, stability, and reproducibility can be achieved as compared to using a traditional Raman imager. So far there is no report on the application of confocal Raman imaging technology to lateral flow test strip. In the present paper we show that combining our home-made confocal Raman imager and lateral flow immunoassay stripscan quantitatively detect the target protein concentrations as low as pM and $\sim 10^4$ cfu/mL, for biomarkers of COVID-19 and Escherichia coli (E. coli) O157: H7, respectively. The results were compared with commercial test strips, indicating that our confocal Raman imaging analysis can significantly improve the detection level of proteins. In addition, the miniaturization of confocal Raman imaging detection equipment is of great significance for highly sensitive real-time on-site detection.

2. MATERIALS AND METHODS

2.1. Materials and Reagents

Sodium citrate, Chloroauric acid, and Hydroxylamine hydrochloride ($NH_2OH{\cdot}HCI$) were purchased from Shanghai Macklin Biochemical Co., Ltd; Novel coronavirus Pneumonia (2019-nCoV) antigen test kit (colloidal gold method) was provided by Bioscience Diagnostic Technology Co., Ltd; Colloidal Gold Immuno-Chromatographic Kit of Escherichia coli O157: H7 (LR 20711) was provided by Beijing Meizheng Bio-Tech Co., Ltd; Bovine albumin (BSA), Polyethylene glycol-20000 (PEG-20000), Anti-SARS-CoV-2 Nucleocapsid Monoclonal Antibody and 2019-nCoV Nucleocapsid Protein were purchased from Beijing Solarbio Science & Technology Co., Ltd; Alexa Fluor®, Pacific Blue™, and Pacific Orange™ Antibody Labeling Kit (A20186) was purchased from Thermo Fisher Scientific; Escherichia coli (E. coli) O157: H7 was purchased from Ningbo testobio Co., Ltd; Escherichia coli (E. coli) O157 Antibody was purchased from East Coast Bio-Techs, Inc; Rabbit IgG and Mouse IgG was purchased from Sangon Biotech (Shanghai) Co., Ltd.

2.2. Preparation for Lateral Flow Immunoassay Strip

Preparation of gold nanospheres: 98.9 mL of millipore water was added to the conical flask and placed on a magnetic stirrer. 1 mL of sodium citrate solution (30 mg/mL) was added and heated to boiling under 1200 rpm stirring. Subsequently, 1 mL of chloroauric acid solution (25 mM) was added and reacted for 30 mins in a stirred boiling state. The color of the solution changes from light yellow to purple, and finally to red. The gold seed solution was formed. 37.4 mL of millipore water, 1 mL of gold seed solution, 400 µL of $NH_2OH{\cdot}HCI$ (100 mM) solution and 400 µL of sodium citrate solution (10 mg/mL) were placed in a flask and stirred for 5 mins to achieve uniform mixing. 800 µL chloroauric acid solution (25 mM) was added and stirred continuously for 1 hour to complete the reaction.

The secondary antibodies were coupled with colloidal gold nanospheres. The pH of the colloidal gold solution was adjusted to 8.0 using a 0.2 M K_2CO_3 solution, with 15 µL of antibody (1 mg/mL) added and incubated at 4°C in dark for 1 hour. BSA (20 µL, 20%) and PEG-20000 solutions (10 µL,

10%) were used to block gold nanospheres and stabilize gold labeled antibodies, and the reaction took place at room temperature for 30 mins. The coupling solution was centrifuged at 4°C at 2000 rpm for 15 mins to remove unbound alternating gold nanospheres, and centrifuged at 4°C at 10000 rpm for 30 mins to obtain antibodies coupled with gold nanospheres. 200 μL gold standard working solution was used for reconstitution and stored at 4°C in the dark.

Composition of lateral flow immunoassay strips. This study was based on commercial test strips (Figure 1(a)), with primary antibodies labeling on the T line and quality control fixed on the C line. After adding the sample solution, when two red lines appear on the test strip, it is considered a positive sample, and when only the red line on the C line appears on the test strip, it is considered a negative sample. If the red line on the C line does not appear, regardless of whether the red line appears on the T line, the result is not credible. Based on confocal Raman imaging for lateral flow immunoassay strip: the gold-marking binding pad with gold nanospheres conjugated secondary antibodies and anti-quality control antibody in the original test strip was replaced by a glass-microfiber separator of the same size before use to ensure that the sample solution can flow completely (Figure 1(e)). Figure 1(a) shows the composition of various parts on the originally commercialized test strip, with the secondary antibodies on the C and T lines already coated. Figures 1(b)–(c) show the specific experimental situation of the test strips being added to both positive and negative samples in this study. Au-Raman probe labeled anti-target secondary antibody, Au-anti-quality control antibody and target proteins (or negative samples) with different gradient concentrations were mixed evenly (∼ 100 μL in total) for sample loading. For positive samples, the target in the solution was recognized by Au-Alexa 647 labeled anti-target secondary antibody, and in the detection window area, it is then captured and aggregated by anti-target primary antibody on the NC membrane, forming a sandwich structure. The Au-anti-quality control was captured and aggregated by the quality control on the C line to form a clear red line to determine the credibility of the test strip's results and the two red lines appear on the test strip. For negative samples, Au-Alexa 647 labeled anti-target secondary antibodies cannot be aggregated on the T line, only a red line on the C line. After a certain period of time, the Raman signals from the sandwich immune complexes were characterized under the action of confocal Raman enhanced scattering for quantitative detection.

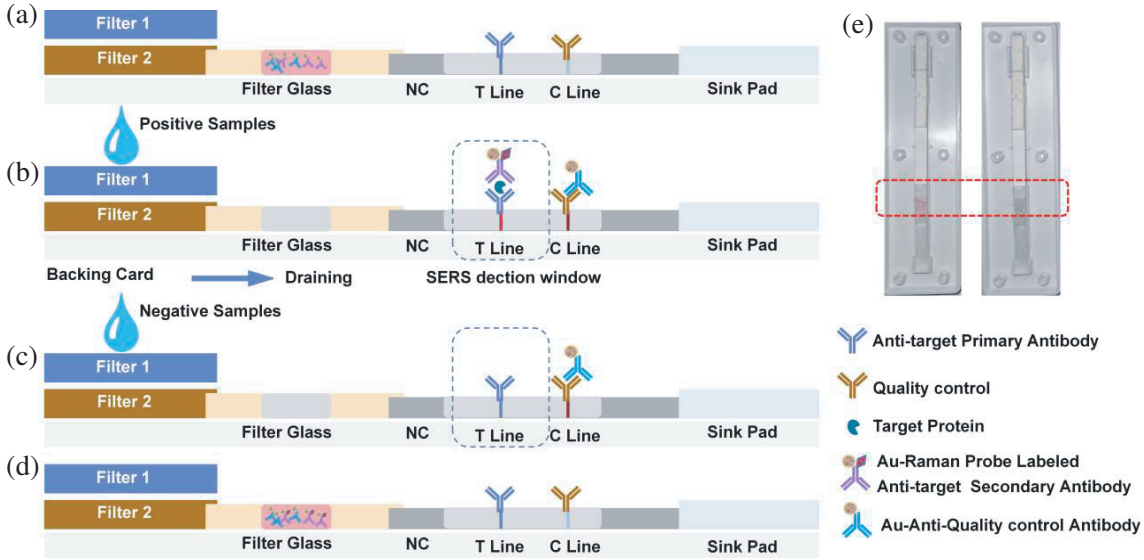

Figure 1. Schematic diagram of the lateral flow immunoassay strip used in this study. (a) The components in each part of the commercial test strip used; Schematic diagram of the test strip in this study when adding (b) positive and (c) negative samples, respectively; (d) The expected composition of the test strip in this study after the test is finished. During testing, only the sample solution needs to be added to complete the reaction; (e) shows the comparison of modifications to commercial test strips in this study. On the left is a commercialized test strip, and on the right is our modified test strip for this experiment.

2.3. Confocal Raman Imaging System

In conventional detection, only single-point Raman signal is usually employed, which may lead to accidental errors. Therefore, in this study we use a home-made confocal Raman microscopy to achieve the spectral acquisition within a range, which includes the spatial distribution information of the sample and the corresponding Raman signal at each point. Combining these two kinds of information, our measurement results are more accurate and reliable. Moreover, the confocal feature of our system can help us filter out the interference information (especially the interference information in the Z-axis direction) the nonfocus area, and further improve the signal-to-noise ratio. As shown in Figure 2, a single-mode fiber-coupled 785 nm laser (FC-D-785-400 mW, Changchun) is collimated by a collimator (F260FC-780) and then injected into the system by a reflector (GCC10220, Daheng Optics, China). A narrow bandpass filter (LL01-785-25; Semrock) is utilized to clean-up the laser. Next, the 785 nm laser beam is reflected by a dichroic mirror (86336, Edmund) and focused on the sample by an objective lens of 10× magnification microscope (Lumplflw series; Olympus Inc). The Raman signal emitted by the sample goes through the objective lens and the dichroic mirror, a long pass edge filter (BLP01-785R-25; Semrock) is used to eliminate the excitation light source, and the dichroic mirror, and then transmits into an aspheric achromatic lens (AL-1, Daheng Optics, China), which is mounted on a z-axis translation mount (SM1Z, Thorlabs). Finally, the Raman signal is focused on a fiber, which is utilized as a pinhole to reject the noise out of focus and is fixed on an SMA fiber adapter plate (SM1SMA, THORLABS), which is assembled on a thread cage plates (CP02/M, THORLABS). The fiber is connected to a fiber-type Raman spectrometer (QE Pro-Raman, Ocean Insight). The upper computer controls the two-dimensional displacement stage (HDS-UH-XY8060SN-RX50-0, Heidstar, China) to realize the laser beam focusing on different areas of the sample. The standard curve is constructed based on different concentrations of targets and corresponding Raman intensities. In this study, 20 points were scanned for each sample to improve the measurement accuracy. We perform at least three parallel measurements on each sample.

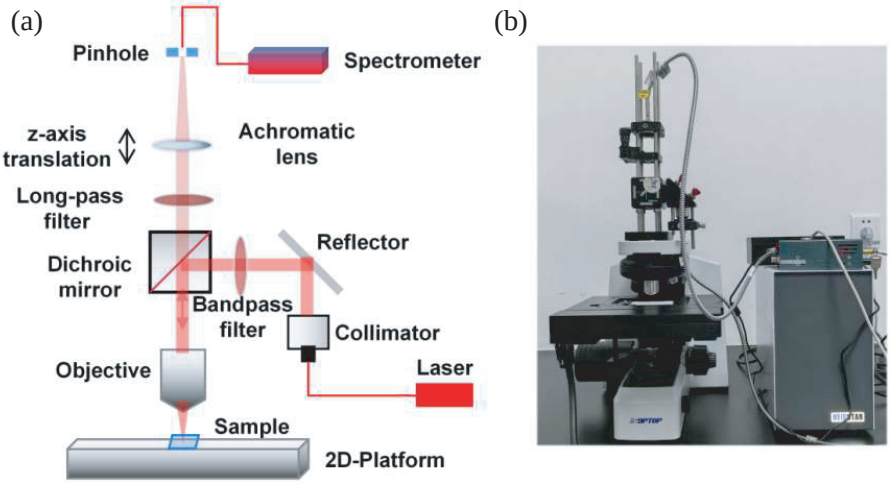

Figure 2. Confocal Raman imaging for the lateral flow immunoassay strip. (a) Schematic diagram of our confocal Raman spectrograph; (b) Photograph of our confocal Raman microscopy.

3. RESULTS AND DISCUSSION

3.1. Characterization of Raman Factor Coupled Complexes

In this study, colloidal gold nanospheres were synthesized using hydroxylamine seed growth method as Raman enhancement factors. The absorption peak results of the generated gold nanospheres are shown in Figure 3(a), showing the maximum absorption peak at ~ 542 nm, indicating a diameter of ~ 60 nm. First, the secondary antibody labeled with Alexa 647 was produced by Alexa fluor antibody labeling

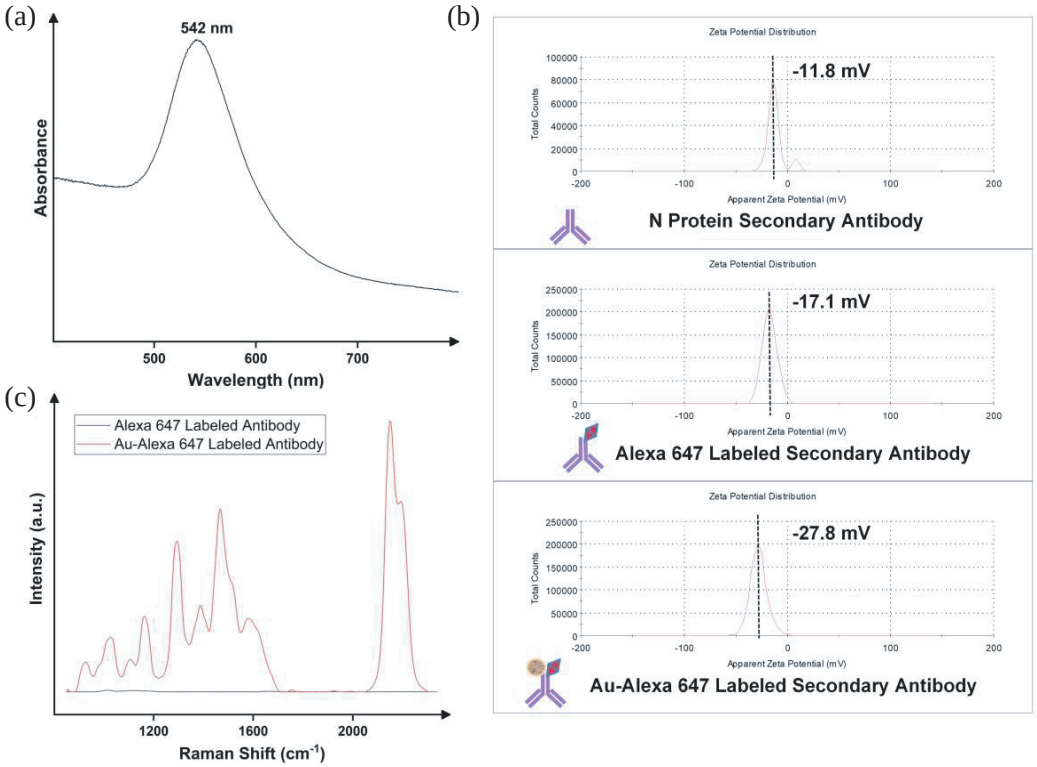

Figure 3. The characterization of each compound in the synthesis process of this study. (a) Absorption peak of the synthesized gold nanospheres; (b) The zeta potential of each compound during the sequential binding of secondary antibodies to Alexa 647 and gold nanospheres; (c) Raman spectroscopy of Alexa 647 conjugated secondary antibodies before and after labeling gold nanospheres.

kit completed and purified. Next, gold nanospheres were coupled with secondary antibodies through electrostatic adsorption. Subsequently, the conjugates of each step in the synthesis were subjected to Zeta potential analysis to determine whether they are coupled. As shown in Figure 3(b), the Zeta potentials of the conjugates were sequentially measured to be −11.8 mV, −17.1 mV, and −27.8 mV, respectively, indicating that gold nanospheres and Alexa 647 have been successfully labeled on anti-N protein secondary antibodies. The compounds before and after the binding of gold nanospheres were subjected to Raman imaging analysis. The Raman spectra in Figure 3(c) shows that under 785 nm excitation, gold nanospheres can significantly enhance Raman scattering. These characteristic results confirm the sensitivity and stability of surface enhanced Raman scattering in quantitative immune detection. In addition, Au-Alexa 647 labeled secondary antibodies of E. coli O157 were also coupled as described above.

3.2. Test for COVID-19 Nucleocapsid Protein

In 2019, the sudden outbreak of COVID-19 brought challenges to the global medical system and COVID-19 continues today. The symptoms of COVID-19 are very similar to the initial symptoms of other seasonal infectious diseases, and it is highly contagious and can be transmitted through direct contact and respiration [55–57]. Therefore, rapid identification of different types of viruses is crucial for preventing virus transmission and providing correct treatment for patients. Although the nucleic acid detection and computed tomography imaging are the gold standard for the COVID-19 diagnosis [58], the sensitivity and accuracy can also meet the needs of sudden outbreaks [59, 60]. However, these methods have some drawbacks in rapid screening in the early and asymptomatic stages of the disease, requiring long testing time, specific testing locations, professional medical staff, and expensive testing equipment. Therefore, real-time serological detection of COVID-19 is needed to supplement the array of clinical diagnosis methods.

We perform our lateral flow immunoassay strip based on confocal Raman imaging on the diagnosis of COVID-19, and nucleocapsid protein was used as the target detector because of its high stability. Anti-nucleocapsid protein (N protein) antibody was used as the primary antibody, Au-Alexa 647 labeled anti-N protein monoclonal antibody was used as the secondary antibody, goat anti-rabbit antibody and Au-rabbit IgG were used as the quality control and anti-quality control, respectively. Different concentrations of N proteins were used for lateral flow immunoassay strip based on confocal Raman imaging. As shown in Figure 4(b), the Raman intensity at wavenumber shift 2156 cm^{-1} is positively correlated with the concentration of N protein. Figure 4(a) shows the Raman intensity at 20 sampling points in the middle of the T line (with the central 10 points on the T line while 5 points on each neighboring side of the T line) by our confocal Raman microscopy when the N protein concentration is 4.74 ng/mL. The standard calibration curve was constructed using N protein with different gradient concentrations and corresponding Raman intensities at 2156 cm^{-1}. The average of ten blank values plus three standard deviations was calculated to obtain a LOD value of 92 pg/mL (Figure 4(c)). And the relative standard deviation (RSD) of the analysis for each N protein gradient concentration is less than $\sim 9\%$, indicating that the method has good precision.

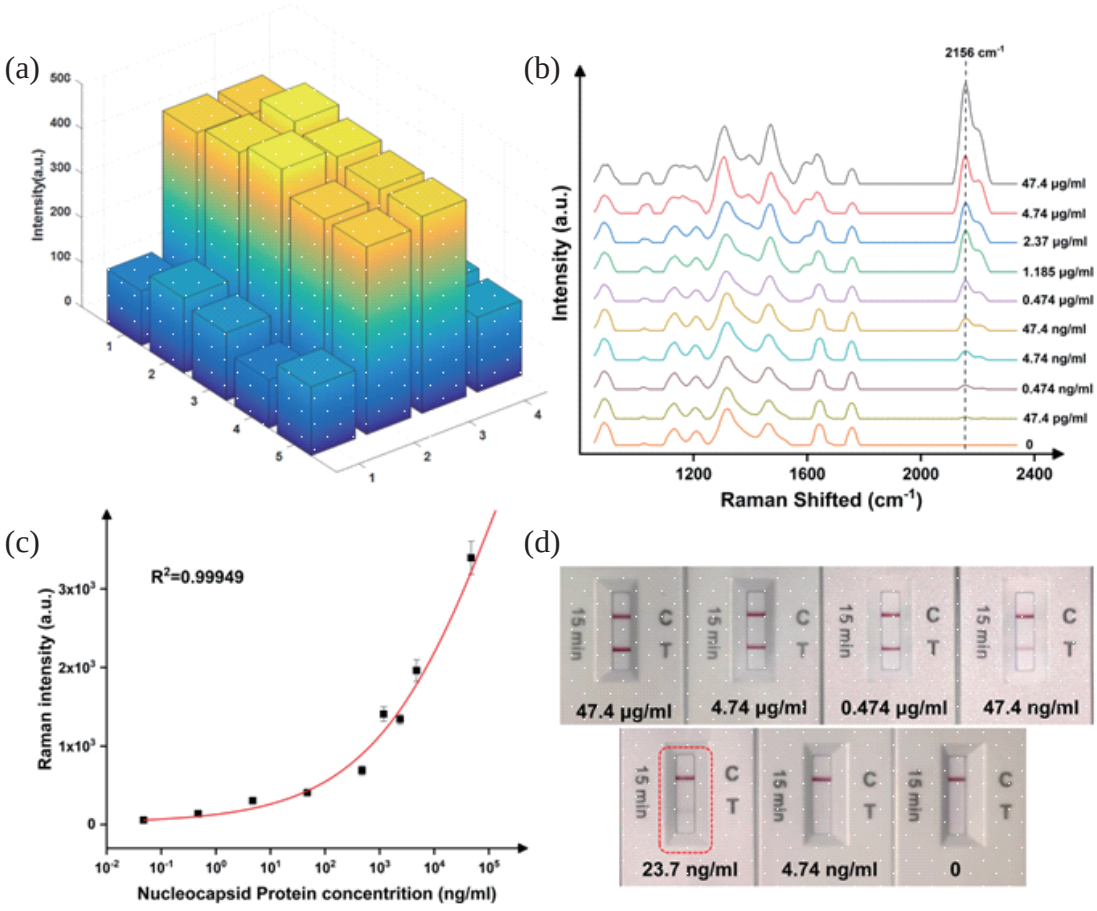

Figure 4. Detection results of COVID-19 N protein by the lateral flow test strip. (a) The Raman intensities at 20 sampling points in the middle of the T line (with the central 10 points on the T line while 5 points on each neighboring side of the T line) when the concentration of N protein is 4.74 ng/mL; (b) Raman spectra and (c) standard curve were established for analysis of N proteins with different gradient concentrations (47.4 μg/mL, 4.74 μg/mL, 2.37 μg/mL, 1.185 μg/mL, 0.474 μg/mL, 47.4 ng/mL, 4.74 ng/mL, 0.474 ng/mL, 47.4 pg/mL and blank), and the error bars are the standard deviation of three repeated experiments using our confocal Raman microscopy; (d) Colorimetric results of commercial test strips of N protein at different concentrations.

In order to evaluate the performance of the lateral flow immunoassay strip based on confocal Raman imaging, this study was compared with commercial colloidal gold test strips, as shown in Figure 4(d). As the concentration of N protein continued to decrease, the color on the T line gradually became lighter while the color on the C line remains unchanged. According to visual observation, when the concentration of N protein is 23.7 ng/mL, the T line basically disappears. In contrast, the lateral flow immunoassay strip in this study based on confocal Raman imaging has much higher sensitivity, improving by two orders of magnitude. This demonstrates the advantages of confocal Raman imaging technique in enhancing the SERS signal sensitivity and uniformity, as well as reducing the background noise and stray light interference. Note that the comparison of the detection sensitivity for different methods is fair and consistent as all of them were applied in the same buffer (or the same sample solutions). The Raman probe used in this study has some characteristic peak located in the Raman silent region, which can avoid the influence of other molecules. Through such Raman signals, the detection specificity and accuracy are improved. Therefore, the lateral flow immunoassay strip based on confocal Raman imaging developed in this study has great potential for rapid, sensitive and quantitative detection of N protein and other biomarkers.

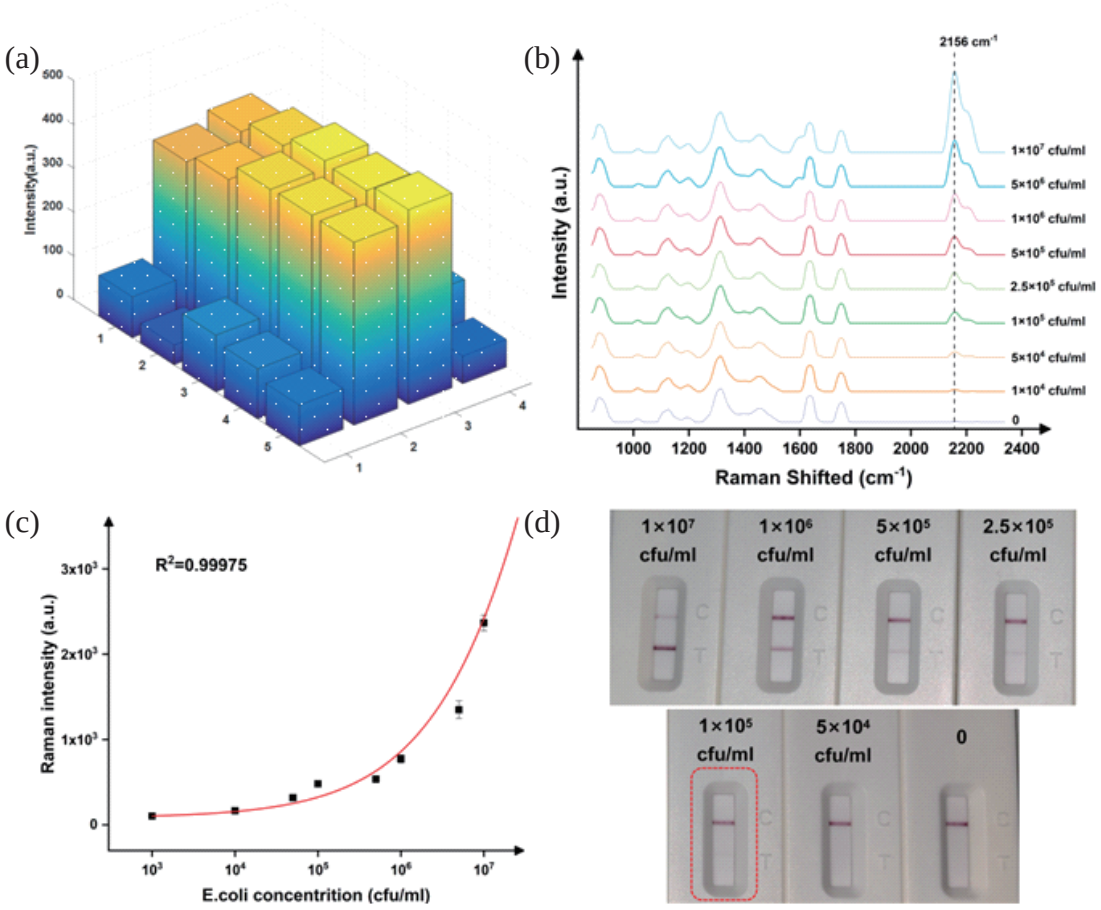

Figure 5. Detection results of E. coli O157: H7 by lateral flow test strip. (a) The Raman intensities at 20 sampling points in the middle of the T line (with the central 10 points on the T line while 5 points on each neighboring side of the T line) when the concentration of E. coli O157: H7 is 5×10^4 cfu/mL; Raman spectra (b) and standard curve (c) were established for analysis of E. coli O157: H7 with different gradient concentrations (1×10^7 cfu/mL, 5×10^6 cfu/mL, 1×10^6 cfu/mL, 5×10^5 cfu/mL, 2.5×10^5 cfu/mL, 1×10^5 cfu/mL, 5×10^4 cfu/mL, 1×10^4 cfu/mL and blank), the error bars are the standard deviation of three repeated experiments; (d) Colorimetric results of commercial test strips of E. coli O157: H7 at different concentrations.

3.3. Test for Escherichia coli O157: H7

In this study we selected E. coli O157: H7 as the detection target to further validate the universality of the test strip based on confocal Raman imaging. E. coli O157: H7 is a human pathogen that is infectious and produces Shiga toxin, often present in foods such as milk, meat, vegetables, or fruits, leading to food poisoning and serious diseases, posing a huge threat to public health [61–63]. Rapid and accurate identification is the key to fundamentally ensuring food safety and preventing the spread of this pathogen. Traditional microbial culture detection and polymerase chain reaction (PCR) are standard methods for detecting E. coli O157: H7 [64]. However, these technologies have high requirements for the professional skills, testing duration, and working environment [65–67]. Traditional microbial cultivation requires sterile operations during the operation process and several days of bacterial cultivation. PCR also requires sample preprocessing and thermal cycle amplification, and is prone to errors such as false positives. This is challenging for real-time analysis. Therefore, developing simple, fast, and high sensitive quantitative detection of microorganisms is very important [68].

For the testing of E. coli O157: H7, anti-E. coli O157: H7 antibody and Au-Alexa 647 labeled E. coli O157 antibody were selected as primary and secondary antibodies, while goat anti-mouse antibody and Au-mouse IgG were selected as the quality control and anti-quality control, respectively. The remaining steps were consistent with Section 2.2 above. Figure 5(a) shows the Raman intensities of 20 sampling points (with the central 10 points on the T line while 5 points on each neighboring side of the T line) by our confocal Raman microscopy when the concentration of E. coli O157: H7 is 5×10^4 cfu/mL. A standard calibration curve was established with different gradient concentrations of E. coli O157: H7 and the corresponding Raman intensities at 2156 cm^{-1} (Figures 5(b)–(c)), and the LOD was determined to be $\sim 1 \times 10^4$ cfu/mL by adding three standard deviations on the average of ten blank values. The RSD of the analysis for each group of E. coli O157: H7 is less than $\sim 7.8\%$, indicating that the analysis has good precision. Figure 5(d) shows a commercial colloidal gold test kit for E. coli O157: H7. In this commercial test strip, Au labeled E. coli O157 antibody was used for aggregation on both the C line and T line simultaneously. So, when the concentration of the E. coli O157 in the sample is high, most of the Au labeled E. coli O157 antibodies were captured by the T line, resulting in a lighter color of the C line and when the concentration of the E. coli O157 in the sample is low, the color on the C line remains consistent. According to visual observation, the color of the T-line gradually disappears when the concentration of E. coli O157: H7 is 1×10^5 cfu/mL. Compared with the results of commercial colloidal gold test kit, the sensitivity of the present method using confocal Raman microscopy is one order of magnitude better. The sensitivity can be improved further by selecting appropriate antibody pairs in the future as commercial antibody pairs are always well optimized.

4. DISCUSSION AND CONCLUSION

In this study, we have developed a lateral flow immunoassay strip based on confocal Raman imaging for quantitative detection of COVID-19 and Escherichia coliO157: H7. Using ordinary gold nanospheres as Raman enhancement factors and fluorescent dyes Alexa 647 to get Raman signals of strong signal noise ratio in the Raman silent region of 1800 cm^{-1} and 2800 cm^{-1}, the detection limit of $\sim 1 \times 10^4$ cfu/mL for E. coli O157: H7 and $\sim$ pM level for N protein have been achieved. Compared with commercial colloidal gold test strips, the detection limit of this technology has been increased by 1-2 orders of magnitude, proving that gold nanospheres can significantly enhance the Raman intensity of target molecules in the lateral flow immunoassay strip. The limit of detection can be improved further if the gold nanospheres are replaced by gold nanorods [69] of suitable aspect ratio or hollow Au nanoshells [70] to give a larger Raman enhancement factor. In addition, in this paper the antibody pairs used for the commercial test strips were the best combination after multiple optimization choices. However, the adaptability of the antibody pairs used in our confocal Raman microscopy experiment was not optimized, and therefore, the improvement of the detection sensitivity in our confocal Raman microscopy experiment could be much greater if the lateral flow immunoassay strip was made professionally instead of made by ourselves non-professionally. If we use antibody pairs from commercial test strips for experiments, the detection sensitivity should be even much better. The experiment is mainly for proof-of-principle demonstration. The entire detection process can be completed within 15 mins, greatly improving detection efficiency. The home-made confocal Raman equipment was used here simply to prove the concept in this paper, and

its size can be reduced significantly to make the system portable. The combination of confocal Raman imaging with lateral flow immunoassay strip to achieve high sensitivity and rapid real-time detection of target proteins, as demonstrated in this paper, is particularly important for screening infectious diseases and detecting bacterial pathogens.

AUTHOR CONTRIBUTIONS

C.Z. performed most of the experiments and prepared the draft. A.Q.Y. made the Raman imaging detection. S.H. designed the research and provided supervision and resources. C.Z. wrote the first draft of the manuscript, which was finalized by S.H. All authors contributed to the revision of this manuscript.

ACKNOWLEDGMENT

This research was funded by 'Pioneer' and 'Leading Goose' R&D Program of Zhejiang Province (grant number 2023C03083 and 2023C03135), the National Key Research and Development Program of China (Grant No. 2022YFC3601000), and National Natural Science Foundation of China (Grant No.11621101). The authors are grateful to Dr. Zhengliang Zhi, and Dr. Julian Evans of Zhejiang University for valuable discussions.

CONFLICTS OF INTEREST

The authors declare no conflict of interest.

REFERENCES

1. Ray, S., S. K. Patel, V. Kumar, J. Damahe, and S. Srivastava, "Differential expression of serum/plasma proteins in various infectious diseases: Specific or nonspecific signatures," *Proteomics Clin. Appl.*, Vol. 8, 53–72, 2014.
2. Tsurusawa, N., J. Chang, M. Namba, D. Makioka, S. Yamura, K. Iha, Y. Kyosei, S. Watabe, T. Yoshimura, and E. Ito, "Modified ELISA for ultrasensitive diagnosis," *J. Clin Med.*, Vol. 10, No. 21, 5197, 2021.
3. Chen, H., M. Xiao, J. He, Y. Zhang, Y. Liang, H. Liu, and Z. Zhang, "Aptamer-functionalized carbon nanotube field-effect transistor biosensors for Alzheimer's disease serum biomarker detection," *ACS Sens.*, Vol. 7, 2075–2083, 2022.
4. Devonshire, A., Y. Gautam, E. Johansson, and T. B. Mersha, "Multi-omics profiling approach in food allergy," *World Allergy Organ J.*, Vol. 16, 100777, 2023.
5. Pei, Y., Y. Tong, H. Li, and J. You, "In-situ biological effects, bioaccumulation, and multi-media distribution of organic contaminants in a shallow lake," *J. Hazard Mater.*, Vol. 427, 128143, 2022.
6. Rodriguez, A., F. Burgos-Florez, J. D. Posada, E. Cervera, V. Zucolotto, H. Sanjuan, M. Sanjuan, and P. J. Villalba, "Electrochemical immunosensor for the quantification of S100B at clinically relevant levels using a cysteamine modified surface," *Sensors (Basel)*, Vol. 21, No. 6, 1929, 2021.
7. Mao, C., S. Wang, Y. Su, S. Tseng, L. He, A. Wu, R. Roden, J. Xiao, and C. Hung, "Protein detection in blood with single-molecule imaging," *Sci. Adv.*, Vol. 7, eabg6522, 2021.
8. Ying, L. and Q. Wang, "Microfluidic chip-based technologies emerging platforms for cancer diagnosis," *BMC Biotechnology*, Vol. 13, 76, 2013.
9. Dijkstra, M. and R. C. Jansen, "Optimal analysis of complex protein mass spectra," *Proteomics.*, Vol. 9, 3869–76, 2009.
10. Roy, P., C. Truntzer, D. Maucort-Boulch, T. Jouve, and N. Molinari, "Protein mass spectra data analysis for clinical biomarker discovery: A global review," *Brief Bioinform.*, Vol. 12, 176–86, 2011.
11. Xu, Z., Y. Jiang, and S. He, "Multi-mode microscopic hyperspectral imager for the sensing of biological samples," *Applied Sciences*, Vol. 10, No. 14, 4876, 2020.

12. Xu, Z., E. Forsberg, Y. Guo, F. Cai, and S. He, "Light-sheet microscopy for surface topography measurements and quantitative analysis," *Sensors*, Vol. 20, No. 10, 2842, 2020.
13. Wang, X., P. Wen, Z. G. Sun, C. Y. Xing, and Y. Li, "Combination of chest CT and clinical features for diagnosis of 2019 novel coronavirus pneumonia," *Open Med. (Wars)*, Vol. 15, 723–727, 2020.
14. Fang, Y., "Large-scale national screening for coronavirus disease 2019 in China," *J. Med. Virol.*, Vol. 92, 2266–2268, 2020.
15. McLaughlin, J. B., B. D. Gessner, T. V. Lynn, E. A. Funk, and J. P. Middaugh, "Association of regulatory issues with an echovirus 18 meningitis outbreak at a children's summer camp in Alaska," *Pediatr. Infect. Dis. J.*, Vol. 23, 875–7, 2004.
16. Sampaio, V. V., A. S. O. Melo, A. L. Coleman, F. Yu, S. R. Martins, L. P. Rabello, J. S. Tavares, and K. Nielsen-Saines, "A novel radiologic finding to predict ophthalmic abnormalities in children with congenital Zika syndrome," *Pediatric. Infect. Dis. Soc. J.*, Vol. 10, 730–737, 2021.
17. Banerjee, R. and A. Jaiswal, "Recent advances in nanoparticle-based lateral flow immunoassay as a point-of-care diagnostic tool for infectious agents and diseases," *Analyst*, Vol. 143, 1970–1996, 2018.
18. Nguyen, V. T., S. Song, S. Park, and C. Joo, "Recent advances in high-sensitivity detection methods for paper-based lateral-flow assay," *Biosens. Bioelectron.*, Vol. 152, 112015, 2020.
19. Li, F., M. You, S. Li, J. Hu, C. Liu, Y. Gong, H. Yang, and F. Xu, "Paper-based point-of-care immunoassays: Recent advances and emerging trends," *Biotechnol. Adv.*, Vol. 39, 107442, 2020.
20. Huang, X., Z. P. Aguilar, H. Xu, W. Lai, and Y. Xiong, "Membrane-based lateral flow immunochromatographic strip with nanoparticles as reporters for detection: A review," *Biosens. Bioelectron.*, Vol. 75, 166–80, 2016.
21. Fu, E., T. Liang, J. Houghtaling, S. Ramachandran, S. A. Ramsey, B. Lutz, and P. Yager, "Enhanced sensitivity of lateral flow tests using a two-dimensional paper network format," *Anal. Chem.*, Vol. 83, 7941–6, 2011.
22. Di Nardo, F., M. Chiarello, S. Cavalera, C. Baggiani, and L. Anfossi, "Ten years of lateral flow immunoassay technique applications: Trends, challenges and future perspectives," *Sensors (Basel)*, Vol. 21, No. 15, 5185, 2021.
23. Rivas, L., A. D. L. Escosura-Muñiz, J. Pons, and A. Merkoçi, "Lateral flow biosensors based on gold nanoparticles," *Gold Nanoparticles in Analytical Chemistry*, 569–605, 2014.
24. Anfossi, L., F. Di Nardo, A. Russo, S. Cavalera, C. Giovannoli, G. Spano, S. Baumgartner, K. Lauter, and C. Baggiani, "Silver and gold nanoparticles as multi-chromatic lateral flow assay probes for the detection of food allergens," *Anal. Bioanal. Chem.*, Vol. 411, 1905–1913, 2019.
25. Wu, J. L., W. P. Tseng, C. H. Lin, T. F. Lee, M. Y. Chung, C. H. Huang, S. Y. Chen, P. R. Hsueh, and S. C. Chen, "Four point-of-care lateral flow immunoassays for diagnosis of COVID-19 and for assessing dynamics of antibody responses to SARS-CoV-2," *J. Infect.*, Vol. 81, 435–442, 2020.
26. Kim, K., L. Kashefi-Kheyrabadi, Y. Joung, K. Kim, H. Dang, S. G. Chavan, M. H. Lee, and J. Choo, "Recent advances in sensitive surface-enhanced Raman scattering-based lateral flow assay platforms for point-of-care diagnostics of infectious diseases," *Sens. Actuators B: Chem.*, Vol. 329, 129214, 2021.
27. Xiang, T., Z. Jiang, J. Zheng, C. Lo, H. Tsou, G. Ren, J. Zhang, A. Huang, and G. Lai, "A novel double antibody sandwich-lateral flow immunoassay for the rapid and simple detection of hepatitis C virus," *Int. J. Mol. Med.*, Vol. 30, 1041–7, 2012.
28. Shi, Z., Y. Tian, X. Wu, C. Li, and L. Yu, "A one-piece lateral flow impedimetric test strip for label-free clenbuterol detection," *Analytical Methods*, Vol. 7, 4957–4964, 2015.
29. Ganguly, A., T. Ebrahimzadeh, P. Zimmern, N. De Nisco, and S. Prasad, "Label free, lateral flow prostaglandin E2 electrochemical immunosensor for urinary tract infection diagnosis," *Chemosensors*, Vol. 9, 271, 2021.

30. Li, Z., Y. Wang, J. Wang, Z. Tang, J. G. Pounds, and Y. Lin, "Rapid and sensitive detection of protein biomarker using a portable fluorescence biosensor based on quantum dots and a lateral flow test strip," *Analytical Chemistry*, Vol. 82, 7008–7014, 2010.
31. Fang, B., S. Hua, C. Wang, M. Yuan, Z. Huang, K. Xing, D. Liu, J. Peng, and W. Lai, "Lateral flow immunoassays combining and colorimetry-fluorescence quantitative detection of sulfamethazine in milk based on trifunctional magnetic nanobeads," *Food Control*, Vol. 98, 268–273, 2019.
32. Wang, Y., C. Fill, and S. R. Nugen, "Development of chemiluminescent lateral flow assay for the detection of nucleic acids," *Biosensors (Basel)*, Vol. 2, 32–42, 2012.
33. Park, J. M., H. W. Jung, Y. W. Chang, H. S. Kim, M. J. Kang, and J. C. Pyun, "Chemiluminescence lateral flow immunoassay based on Pt nanoparticle with peroxidase activity," *Anal. Chim. Acta.*, Vol. 853, 360–367, 2015.
34. Khlebtsov, B. and N. Khlebtsov, "Surface-enhanced Raman scattering-based lateral-flow immunoassay," *Nanomaterials (Basel)*, Vol. 10, No. 11, 2228, 2020.
35. Gunawardhana, L., K. Kourentzi, A. Danthanarayana, J. Brgoch, X. Shan, R. Willson, and W. Shih, "SERS-based ultrasensitive lateral flow assay for quantitative sensing of protein biomarkers," *IEEE Journal of Selected Topics in Quantum Electronics*, Vol. 27, 6900608, 2021.
36. Chen, S., L. Meng, L. Wang, X. Huang, S. Ali, X. Chen, M. Yu, M. Yi, L. Li, X. Chen, L. Yuan, W. Shi, and G. Huang, "SERS-based lateral flow immunoassay for sensitive and simultaneous detection of anti-SARS-CoV-2 IgM and IgG antibodies by using gap-enhanced Raman nanotags," *Sens. Actuators B: Chem.*, Vol. 348, 130706, 2021.
37. Tran, V., B. Walkenfort, M. Konig, M. Salehi, and S. Schlucker, "Rapid, quantitative, and ultrasensitive point-of-care testing: A portable SERS reader for lateral flow assays in clinical chemistry," *Angew. Chem. Int. Ed. Engl.*, Vol. 58, 442–446, 2019.
38. Sloan-Dennison, S., E. O'Connor, J. W. Dear, D. Graham, and K. Faulds, "Towards quantitative point of care detection using SERS lateral flow immunoassays," *Anal. Bioanal. Chem.*, Vol. 414, 4541–4549, 2022.
39. Lia, Y., S. Tang, W. Zhang, X. Cui, Y. Zhang, Y. Jin, X. Zhang, and Y. Chen, "A surface-enhanced Raman scattering-based lateral flow immunosensor for colistin in raw milk," *Sens. Actuators B: Chem.*, Vol. 282, 703–711, 2019.
40. Jones, R. R., D. C. Hooper, L. Zhang, D. Wolverson, and V. K. Valev, "Raman techniques: Fundamentals and frontiers," *Nanoscale Res. Lett.*, Vol. 14, 231, 2019.
41. Ando, J. and K. Fujita, "Metallic nanoparticles as SERS agents for biomolecular imaging," *Current Pharmaceutical Biotechnology*, Vol. 14, 141–149, 2013.
42. Bantz, K. C., A. F. Meyer, N. J. Wittenberg, H. Im, O. Kurtulus, S. H. Lee, N. C. Lindquist, S. H. Oh, and C. L. Haynes, "Recent progress in SERS biosensing," *Phys. Chem. Chem. Phys.*, Vol. 13, 11551–67, 2011.
43. Chen, R., X. Du, Y. Cui, X. Zhang, Q. Ge, J. Dong, and X. Zhao, "Vertical flow assay for inflammatory biomarkers based on nanofluidic channel array and SERS nanotags," *Small*, Vol. 16, e2002801, 2020.
44. Fu, X., Z. Cheng, J. Yu, P. Choo, L. Chen, and J. Choo, "A SERS-based lateral flow assay biosensor for highly sensitive detection of HIV-1 DNA," *Biosens. Bioelectron.*, Vol. 78, 530–537, 2016.
45. Zhang, W., S. Tang, Y. Jin, C. Yang, L. He, J. Wang, and Y. Chen, "Multiplex SERS-based lateral flow immunosensor for the detection of major mycotoxins in maize utilizing dual Raman labels and triple test lines," *J. Hazard Mater.*, Vol. 393, 122348, 2020.
46. He, D., Z. Wu, B. Cui, and E. Xu, "Dual-mode aptasensor for SERS and Chiral detection of campylobacter jejuni," *Food Analytical Methods*, Vol. 12, 2185–2193, 2019.
47. Su, L., H. Hu, Y. Tian, C. Jia, L. Wang, H. Zhang, J. Wang, and D. Zhang, "Highly sensitive colorimetric/surface-enhanced Raman spectroscopy immunoassay relying on a metallic core-shell Au/Au nanostar with clenbuterol as a target analyte," *Anal. Chem.*, Vol. 93, 8362–8369, 2021.

48. Liu, B., S. Zheng, Q. Liu, B. Gao, X. Zhao, and F. Sun, "SERS-based lateral flow immunoassay strip for ultrasensitive and quantitative detection of acrosomal protein SP10," *Microchemical Journal*, Vol. 175, 107191, 2022.
49. He, W., M. Wang, M. Li, Z. Zhong, H. Chen, S. Xi, Z. Luan, C. Li, and X. Zhang, "Confocal Raman microscopy for assessing effects of preservation methods on symbiotic deep-sea mussel gills," *Frontiers in Marine Science*, Vol. 9, 2022.
50. Hu, C., X. Wang, L. Liu, C. Fu, K. Chu, and Z. J. Smith, "Fast confocal Raman imaging via context-aware compressive sensing," *The Analyst*, Vol. 146, 2348–2357, 2021.
51. Guo, T., Z. Lin, X. Xu, Z. Zhang, X. Chen, N. He, G. Wang, Y. Jin, J. Evans, and S. He, "Dichroic metagrating Fabry-Perot filter based on liquid crystal for spectral imaging," *Progress In Electromagnetics Research*, Vol. 177, 43–51, 2023.
52. Luo, J., Z. Lin, Y. Xing, E. Forsberg, C. Wu, X. Zhu, T. Guo, G. Wang, B. Bian, D. Wu, and S. He, "Portable 4D snapshot hyperspectral imager for fastspectral and surface morphology measurements," *Progress In Electromagnetics Research*, Vol. 173, 25–36, 2022.
53. Jiao, C., Z. Lin, Y. Xu, and S. He, "Noninvasive raman imaging for monitoring mitochondrial redox state in septic rats," *Progress In Electromagnetics Research*, Vol. 175, 149–157, 2022.
54. Paddock, S., "Principles and practices of laser scanning confocal microscopy," *Molecular Biotechnology*, Vol. 16, 127–149, 2000.
55. Vos, T., A. D. Flaxman, M. Naghavi, R. Lozano, C. Michaud, and M. Ezzati, "Years lived with disability (YLDs) for 1160 sequelae of 289 diseases and injuries 1990–2010: A systematic analysis for the Global Burden of Disease Study 2010," *Lancet*, Vol. 380, 2163–96, 2012.
56. Park, S. W., D. M. Cornforth, J. Dushoff, and J. S. Weitz, "The time scale of asymptomatic transmission affects estimates of epidemic potential in the COVID-19 outbreak," *Epidemics*, Vol. 31, 100392, 2020.
57. Li, Q., X. Guan, P. Wu, X. Wang, L. Zhou, Y. Tong, R. Ren, K. S. M. Leung, E. H. Y. Lau, J. Y. Wong, X. Xing, N. Xiang, Y. Wu, C. Li, Q. Chen, D. Li, T. Liu, J. Zhao, M. Liu, W. Tu, C. Chen, L. Jin, R. Yang, Q. Wang, S. Zhou, R. Wang, H. Liu, Y. Luo, Y. Liu, G. Shao, H. Li, Z. Tao, Y. Yang, Z. Deng, B. Liu, Z. Ma, Y. Zhang, G. Shi, T. T. Y. Lam, J. T. Wu, G. F. Gao, B. J. Cowling, B. Yang, G. M. Leung, and Z. Feng, "Early transmission dynamics in Wuhan, China, of novel coronavirus-infected pneumonia," *N. Engl. J. Med.*, Vol. 382, 1199–1207, 2020.
58. Li, Z., Y. Yi, X. Luo, N. Xiong, Y. Liu, S. Li, R. Sun, Y. Wang, B. Hu, W. Chen, Y. Zhang, J. Wang, B. Huang, Y. Lin, J. Yang, W. Cai, X. Wang, J. Cheng, Z. Chen, K. Sun, W. Pan, Z. Zhan, L. Chen, and F. Ye, "Development and clinical application of a rapid IgM-IgG combined antibody test for SARS-CoV-2 infection diagnosis," *J. Med. Virol.*, Vol. 92, 1518–1524, 2020.
59. Zhou, Y., L. Zhang, Y. H. Xie, and J. Wu, "Advancements in detection of SARS-CoV-2 infection for confronting COVID-19 pandemics," *Lab Invest.*, Vol. 102, 4–13 2022.
60. Vega-Magana, N., R. Sanchez-Sanchez, J. Hernandez-Bello, A. A. Venancio-Landeros, M. Pena-Rodriguez, R. A. Vega-Zepeda, B. Galindo-Ornelas, M. Diaz-Sanchez, M. Garcia-Chagollan, G. Macedo-Ojeda, O. P. Garcia-Gonzalez, and J. F. Munoz-Valle, "RT-qPCR assays for rapid detection of the N501Y, 69-70del, K417N, and E484K SARS-CoV-2 mutations: A screening strategy to identify variants with clinical impact," *Front Cell Infect Microbiol.*, Vol. 11, 672562, 2021.
61. Croxen, M. A., R. J. Law, R. Scholz, K. M. Keeney, M. Wlodarska, and B. B. Finlay, "Recent advances in understanding enteric pathogenic Escherichia coli," *Clin. Microbiol. Rev.*, Vol. 26, 822–80, 2013.
62. Pennington, H., "Escherichia coli O157," *Lancet*, Vol. 376, 1428–35, 2010.
63. Song, C., C. Liu, S. Wu, H. Li, H. Guo, B. Yang, S. Qiu, J. Li, L. Liu, H. Zeng, X. Zhai, and Q. Liu, "Development of a lateral flow colloidal gold immunoassay strip for the simultaneous detection of Shigella boydii and Escherichia coli O157 H7 in bread, milk and jelly samples," *Food Control*, Vol. 59, 345–351, 2016.
64. Pang, B., C. Zhao, L. Li, X. Song, K. Xu, J. Wang, Y. Liu, K. Fu, H. Bao, D. Song, X. Meng, X. Qu, Z. Zhang, and J. Li, "Development of a low-cost paper-based ELISA method for rapid Escherichia coli O157: H7 detection," *Anal. Biochem.*, Vol. 542, 58–62, 2018.

65. Zhao, Y., Y. Li, P. Zhang, Z. Yan, Y. Zhou, Y. Du, C. Qu, Y. Song, D. Zhou, S. Qu, and R. Yang, "Cell-based fluorescent microsphere incorporated with carbon dots as a sensitive immunosensor for the rapid detection of Escherichia coli O157 in milk," *Biosens. Bioelectron.*, Vol. 179, 113057, 2021.
66. Li, Z., X. Zhang, H. Qi, X. Huang, J. Shi, and X. Zou, "A novel renewable electrochemical biosensor based on mussel-inspired adhesive protein for the detection of Escherichia coli O157 H7 in food," *Sens. Actuators B: Chem.*, Vol. 372, 132601, 2022.
67. Jo, Y., J. Park, and J. K. Park, "Colorimetric detection of escherichia coli O157: H7 with signal enhancement using size-based filtration on a finger-powered microfluidic device," *Sensors (Basel)*, Vol. 20, No. 8, 2267, 2020.
68. Sun, Y., C. Kuo, C. Lu, and C. Lin, "Review of recent advances in improved lateral flow immunoassay for the detection of pathogenic Escherichia coli O157 H7 in foods," *Journal of Food Safety*, Vol. 41, e12867, 2021.
69. Nikoobakht, B. and M. A. El-Sayed, "Surface-enhanced Raman scattering studies on aggregated gold nanorods," *J. Phys. Chem. A.*, Vol. 107, 3372–3378, 2003.
70. Farooq, S. and R. E. de Araujo, "Identifying high performance gold nanoshells for singlet oxygen generation enhancement," *Photodiagnosis and Photodynamic Therapy*, Vol. 35, 102466, 2021.